JOURNAL OF VIROLOGY, Dec. 2005, p. 15016–15026 Vol. 79, No. 24
0022-538X/05/$08.00+0 doi:10.1128/JVI.79.24.15016–15026.2005

A Point Mutation within the Replicase Gene Differentially Affects Coronavirus Genome versus Minigenome Replication

Carmen Galán, Luis Enjuanes,* and Fernando Almazán

Centro Nacional de Biotecnología, CSIC, Department of Molecular and Cell Biology, Campus Universidad Autónoma, Cantoblanco, Darwin St. 3, 28049 Madrid, Spain

Received 13 June 2005/Accepted 20 September 2005

During the construction of the *transmissible gastroenteritis virus* (TGEV) full-length cDNA clone, a point mutation at position 637 that was present in the defective minigenome DI-C was maintained as a genetic marker. Sequence analysis of the recovered viruses showed a reversion at this position to the original virus sequence. The effect of point mutations at nucleotide 637 was analyzed by reverse genetics using a TGEV full-length cDNA clone and cDNAs from TGEV-derived minigenomes. The replacement of nucleotide 637 of TGEV genome by a T, as in the DI-C sequence, or an A severely affected virus recovery from the cDNA, yielding mutant viruses with low titers and small plaques compared to those of the wild type. In contrast, T or A at position 637 was required for minigenome rescue in *trans* by the helper virus. No relationship between these observations and RNA secondary-structure predictions was found, indicating that mutations at nucleotide 637 most likely had an effect at the protein level. Nucleotide 637 occupies the second codon position at amino acid 108 of the pp1a polyprotein. This position is predicted to map in the N-terminal polyprotein papain-like proteinase (PLP-1) cleavage site at the p9/p87 junction. Replacement of G-637 by A, which causes a drastic amino acid change (Gly to Asp) at position 108, affected PLP-1-mediated cleavage in vitro. A correlation was found between predicted cleaving and noncleaving mutations and efficient virus rescue from cDNA and minigenome amplification, respectively.

Transmissible gastroenteritis virus (TGEV) is a member of the *Coronaviridae* family, which has recently been grouped with the *Arteriviridae* and the *Roniviridae* in the *Nidovirales* order (7, 14). Coronaviruses are the causative agents of a variety of diseases that impact animal and human health, including newly discovered members, such as the etiologic agent of severe acute respiratory syndrome and the human coronaviruses NL63 and HKU1 (13, 15, 32, 34, 42, 45).

Coronavirus genomes are single-stranded positive-sense infectious RNA molecules, the largest genomes known within RNA viruses, sharing a similar genome organization (4). The replicase gene encompasses the 5′ two thirds of the genome and contains two overlapping open reading frames (ORF1a and ORF1b) that are translated by a ribosomal frameshift mechanism, leading to the expression of two large co-amino-terminal polyproteins, pp1a and pp1ab (5). Controlled proteolysis of these polyproteins by different virus-encoded proteinases regulates the release of the viral components of the replication-transcription complex (46, 47). This complex is believed to perform the synthesis of (i) the genome-size infectious RNA through a minus-strand antigenomic template, (ii) a nested set of subgenomic RNAs by a discontinuous transcription mechanism that most probably occurs during the synthesis of the negative strand (23, 36, 37), and (iii) deleted genomes, referred to as defective interfering RNAs or minigenomes, that conserve the *cis*-acting signals required for their amplification (18, 25, 28, 31, 44). Although RNA signals specifically involved in the synthesis of the subgenomic RNAs have been well characterized (40, 50), possible differences in the machinery involved in the production of the different species of viral RNAs have not been addressed.

Coronavirus-derived minigenomes have been widely used to study different aspects of coronavirus replication. However, little is known about the precise mechanism and the selection pressure controlling their efficient maintenance in a helper-dependent system. Although findings in plant RNA viruses have illustrated some differences in the elements that regulate *trans*-accumulation of minigenomes from those controlling replication of the genomic RNA (33), no systematic studies of the elements controlling coronavirus replication have been reported in the context of both genomic and defective RNAs. The recent availability of coronavirus infectious clones and functional replicons allows reliable evaluation of the replication signals extrapolated from the analysis with defective RNAs.

Coronavirus ORF1a encodes one or two papain-like proteinases (PLPs) that are responsible for cleavage at one or two sites located in the N-proximal region of the replicase. The conservation and activity of the PLP proteinases vary among the three different coronavirus groups. PLP-1 plays a role in proteolytic processing at the relatively divergent amino terminus of the ORF1a polyprotein in coronavirus groups 1 and 2. In group 1 human coronavirus 229E (HCoV-229E), PLP-1 mediates the release of an amino-terminal 9-kDa protein and the adjacent 87-kDa protein, named p9 and p87, respectively (17, 48). The same processing pattern has been predicted by sequence comparison for the closely related TGEV coronavirus. For group 2 coronaviruses, including bovine coronavirus and mouse hepatitis virus (MHV), PLP-1 liberates the N-terminal p28 and p65 proteins of 28 and 65 kDa, respectively (2, 3, 10, 12). Functional explanations for these group-specific divergences have not yet been elucidated. Although PLP-1 cleavage products have been identified in virus-infected cells for MHV and HCoV-229E (17, 39), the specific activity of these proteins remains poorly characterized, and no

* Corresponding author. Mailing address: Department of Molecular and Cell Biology, Centro Nacional de Biotecnología, CSIC, Campus Universidad Autónoma, Cantoblanco. Darwin St. 3, 28049 Madrid, Spain. Phone: 34 91 585 4555. Fax: 34 91 585 4915. E-mail: L.Enjuanes@cnb.uam.es.

TABLE 1. Oligonucleotides used in this study

Oligonucleotide[a]	Method[b]	Oligonucleotide sequence, 5′→3′[c]	Amplicon size (bp)
Oli5′I	PCR 637 mut	AATTCGATGATAAGCTGTCAAC	1,558
Oli3′I	PCR 637 mut	GGCACCTCTG(G/C/T)CAGTGCGAGCAATTTTAAG	
Oli5′D	PCR 637 mut	GCTCGCACTG(A/C/G)CAGAAGGTGCCATATATGTTG	912
Oli3′D	PCR 637 mut	TCCTCTACTACTTTCCAAGCGTC	
Oli5′I	PCR 637 mut	AATTCGATGATAAGCTGTCAAC	2,449
Oli3′D	PCR 637 mut	TCCTCTACTACTTTCCAAGCGTC	
Q-LBS7-VS	Q-RT-PCR M33L	TACCAACACACCATGAAAAAATGC	123
Q-7-RS	Q-RT-PCR M33L	TCATTGACAGTTTTAAGATTGAAAGAGTG	
Q-2060-VS	Q-RT-PCR DI-C	TAAAGTTCCATCTTATGACATCGTTTATG	108
Q-2167-RS	Q-RT-PCR DI-C	TCTTGTGTGCCAGTTGGTATTTG	
KpnI-M-E859-VS	PCR PLP-1	GCGCGGTACC**ATG**GAACATTTTTATCCTTATGG	1,375
BamHI-STOP-S1315-RS	PCR PLP-1	CGCGGGATCC**TTA**ACTTTGAATTTTCCTCTTTTTC	
KpnI-ORF1a-M1-VS	PCR ORF1a-S	GCGCGGTACC**ATG**AGTTCCAAACAATTCAAG	1,830
BamHI-STOP-ORF1a-E610-RS	PCR ORF1a-S	CGCGGGATCC**TTA**TTCAAATGATGAACCAAGTTTTG	

[a] VS, virus sense; RS, reverse sense.
[b] PCR 637 mut, PCR for mutagenesis at position 637; Q-RT-PCR (M33L or DI-C), primers used for the quantification by Q-RT-PCR of the specified minigenome; PCR (PLP-1 or ORF1a), primers used for cloning of TGEV PLP-1 proteinase or substrate, respectively.
[c] The mutated nucleotide is shown in parentheses. Restriction endonuclease sites used for cloning are underlined (KpnI, GGTACC; BamHI, GGATCC); translation initiation (ATG) and termination (TTA) codons are shown in bold.

counterparts of these proteins have been identified in other cellular or viral systems by sequence comparison. The MHV p28 and p65 polypeptides seem to be associated with intracellular membranes and colocalize with viral replication complexes (39). Additionally, it has been demonstrated that the expression of p28 induced cell cycle arrest in G_0/G_1 phase (8). Requirements of p28 and p65 for MHV-A59 replication have been studied by reverse genetics, showing that processing at the amino-terminal cleavage site of the replicase was not strictly essential for viral replication. However, predicted noncleaving mutations severely altered virus growth, protein processing, and RNA synthesis (11). No specific roles or functional requirements have been studied so far for the HCoV-229E or TGEV counterpart proteins p9 and p87.

In the present study, we characterize the effect of a point mutation at position 637 in the TGEV genome, affecting the predicted PLP-1 cleavage site at the p9/p87 junction. A mutational analysis at this position was performed by reverse genetics in the TGEV full-length cDNA clone (1) and in two TGEV-derived minigenomes of different sizes (20). Different nucleotides at position 637 were required for virus recovery from the cDNA and helper-mediated minigenome accumulation. A correlation was found between predicted cleaving and noncleaving mutations and the nucleotides selected for virus and minigenome replication, respectively.

MATERIALS AND METHODS

Cells and viruses. Baby hamster kidney cells stably transformed with the porcine aminopeptidase N gene (BHK-pAPN) (9) were grown in Dulbecco's modified Eagle's medium supplemented with 5% fetal calf serum and geneticin (1.5 mg/ml) as a selection agent. The TGEV PUR46-MAD strain (35) was used as the helper virus in the minigenome rescue system. Wild-type and recombinant viruses were grown and titrated in swine testis (ST) cells (27) as described previously (21).

Plasmid constructs and mutagenesis. To generate TGEV cDNAs with point mutations at genome position 637, the intermediate plasmid pBAC-TGEV (SrfI-NheI) (50) was used as a template for overlapping PCRs. A 1,558-bp PCR fragment, containing the cytomegalovirus promoter and the first 647 nucleotides of the TGEV genome (30) (GenBank accession number AJ271965) with the desired point mutations at position 637, was amplified with oligonucleotides Oli5′I and Oli3′I, described in Table 1. A 912-bp overlapping PCR fragment including nucleotides 627 to 1531 of the TGEV genome with the corresponding mutations was amplified with primers Oli5′D and Oli3′D (Table 1). The final 2,449-bp PCR product was amplified using the overlapping PCR products and the outer oligonucleotides Oli5′I and Oli3′D, digested with SrfI and ApaLI, and cloned into the same restriction sites of plasmid pBAC-TGEV (SrfI-NheI), generating the plasmids pBAC-TGEV(SrfI-NheI)637A, pBAC-TGEV(SrfI-NheI)637T, pBAC-TGEV(SrfI-NheI)637C, and pBAC-TGEV(SrfI-NheI)637G. To introduce the engineered mutations in the TGEV infectious cDNA, the 5,277-bp SrfI-ClaI fragment from pBAC-TGEV(SrfI-NheI) with the corresponding mutation was cloned into the same sites of pBAC-TGEV$^{\Delta ClaI}$ digested with the same restriction enzymes. Finally, the full-length cDNA clone was generated by cloning the ClaI^{4417}-ClaI^{9615} fragment as previously described (1).

The construction of cDNAs encoding TGEV-derived RNA minigenome DI-C (9.7 kb) and DI-C-derived RNA minigenome M33 (3.3 kb) was previously described. These minigenomes were cloned under the T7 promoter and flanked at the 3′ end by the hepatitis delta virus ribozyme (Rz) and the T7 terminator sequence (20). The M33L minigenome was constructed from the M33 minigenome by cloning a heterologous sequence of 16 bp, referred to as the linker, which does not interfere with the efficient rescue of this minigenome.

The original sequence of the DI-C and M33L cDNAs contains a T at position 637. M33L and DI-C cDNAs with point mutations at position 637 were generated by restriction fragment exchange. To get the M33L-637G cDNA, plasmid pBAC-TGEV-5′END, containing nucleotides 1 to 1496 from the TGEV genome, was digested with NaeI and SphI and the resulting 1,047-bp restriction fragment was cloned into the same sites of the plasmid coding for the M33L minigenome (pM33L). Plasmids pM33L-637A and pM33L-637C were generated by cloning the 646-bp NaeI-EcoRV restriction fragment from plasmids pBAC-TGEV(SrfI-NheI)637A and pBAC-TGEV(SrfI-NheI)637C, respectively, into plasmid pM33L digested with the same restriction enzymes.

DI-C cDNAs with point mutations at position 637 were generated by cloning the 1,229-bp NarI-EcoRV restriction fragment from pM33L with the corresponding mutations into the plasmid pDI-C (20) digested with the same restriction enzymes.

For the construction of plasmid pTGEV-PLP-1 encoding the PLP-1 domain, the genomic region corresponding to nucleotides 2889 to 4259, which encodes Glu859 to Ser1315 from pp1a, was amplified from pBAC-TGEV(SrfI-NheI) using primers KpnI-M-E859-VS and BamHI-STOP-S1315-RS, which introduced a KpnI site and a translation initiation codon at the 5′ end and a translation

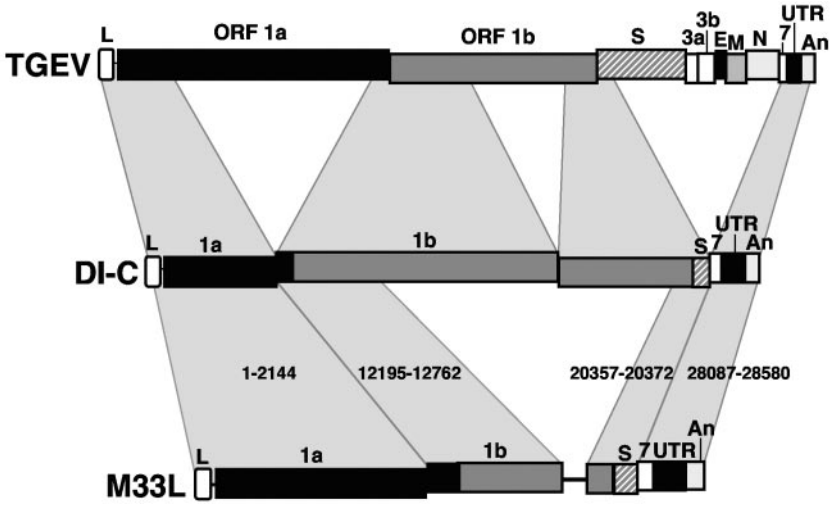

FIG. 1. Genetic structure of the TGEV genome and defective RNAs. The bar on top represents the TGEV virus genome, in which the different genes are depicted as boxes. The sequence relationship between the parental genome and minigenomes DI-C and M33L is indicated by shadowed polygons. The nucleotide positions of each discontinuous region in the TGEV genome are indicated for the minigenome M33L. L, leader; ORF1a and ORF1b, replicase genes; S, spike gene; 3a and 3b, nonstructural 3a and 3b genes; E, envelope protein gene; M, membrane protein gene; N, nucleoprotein gene; 7, nonstructural gene 7; UTR, untranslated region; An, poly(A).

termination codon followed by a BamHI site at the 3′ end (Table 1). Following KpnI and BamHI digestion, a fragment containing the predicted PLP-1 domain was ligated into KpnI- and BamHI-cleaved pcDNA3 (Invitrogen).

For the generation of plasmids pTGEV-ORF1a(637G) and pTGEV-ORF1a(637A), the fragments encoding the N-terminal 610 amino acids from ORF1a, with either Gly or Asp at position 108, were obtained by PCR from plasmid pM33L-637G or pM33L-637A using primers KpnI-ORF1a-M1-VS and BamHI-STOP-ORF1a-E610-RS (Table 1) and cloned into KpnI- and BamHI-digested pcDNA3.

All cloning steps were checked by sequencing the PCR-amplified fragments and cloning junctions.

Transfection and recovery of recombinant viruses from cDNA clones. BHK-pAPN cells were grown to 95% confluence in 35-mm-diameter plates and transfected with 5 μg of each pBAC-TGEV^{FL} plasmid containing the corresponding mutation at position 637 and 12 μg of Lipofectamine 2000 (Invitrogen) in Optimem medium according to the manufacturer's specifications. Cells were incubated at 37°C for 6 h, then the transfection medium was discarded, and the cells were trypsinized and plated over a confluent monolayer of ST cells grown in a 35-mm-diameter plate. Cell supernatants were harvested for titration at 24, 48, and 72 h posttransfection.

In vitro transcription. Capped minigenome transcripts were generated from XhoI-linearized DNA templates using the T7 polymerase mMessage-mMachine kit (Ambion), according to the manufacturer's procedure. The length of the in vitro-transcribed RNAs was analyzed by denaturing 1% agarose-2.2 M formaldehyde gel electrophoresis.

Rescue of minigenomes by RNA transfection of helper virus-infected ST cells. ST cells were grown to 90% confluence and infected with TGEV PUR46-MAD at a multiplicity of infection of 10. At 2 h postinfection, cells were transfected with 1 μg of in vitro-transcribed RNA using 3 μg of Lipofectamine 2000 (Invitrogen) according to the manufacturer's specifications and incubated for 4 h at 37°C. Cells were then washed and incubated with fresh Dulbecco's modified Eagle's medium containing 2% fetal bovine serum. Supernatants from these cultures were used to infect fresh ST cell monolayers at 22 h postinfection and five serial passages were performed to amplify the minigenome RNA. Virus titer was determined in each passage as previously described (21). Total RNA was extracted in each passage by using the RNeasy Mini Kit (QIAGEN) according to the manufacturer's instructions. Additionally, total RNA was extracted at passage zero just after transfection from replicate samples, to further comparison of input minigenome RNA levels by real-time quantitative reverse transcription (RT)-PCR (Q-RT-PCR).

Q-RT-PCR. Analysis of minigenome rescue efficiency was performed by Q-RT-PCR on total RNA from each virus passage. cDNAs were synthesized at 50°C for 90 min with 5 units of Reflectase RT reverse transcriptase (Active Motif) using the antisense primers described in Table 1. The cDNAs generated were used as templates for real-time PCR amplification using specific primer pairs designed with the Primer Express software (Table 1). The designed amplicons encompass specific discontinuous minigenome regions to discriminate hybridization with the viral genome. In the PCR step, SYBR Green master mix (Applied Biosystems) was used according to the manufacturer's specifications. Data acquisition was performed using an ABI PRISM 7000 sequence detection system (Applied Biosystems) and analyzed with ABI PRISM 7000 SDS version 1.0 software. All quantifications were performed in duplicate from two separate RNA transcripts of each minigenome which were transfected and rescued in parallel to validate the experimental data.

In vitro coupled transcription-translation and *trans*-cleavage assay. TGEV PLP-1 proteinase and ORF1a substrates cloned under the control of the T7 promoter were expressed using the TNT T7-coupled reticulocyte lysate system (Promega) according to the manufacturer's instructions. For the preparation of labeled substrates, in vitro transcription-translation reactions from pTGEV-ORF1a(637G) and pTGEV-ORF1a(637A) plasmids were performed in the presence of 20 μCi of L-[^{35}S]methionine (1,000 Ci/mmol at 10 mCi/ml; Amersham) and incubated at 30°C for 90 min. For PLP-1 translation, nonlabeled reactions were carried out in parallel in the presence of 1 mM methionine in accordance with the manufacturer's specifications, except that 100 μM $ZnCl_2$ was added. Following completion of both substrate and enzyme reactions, cycloheximide was added to a final concentration of 0.6 μg/μl to prevent further translation. Then, the substrate reaction mixtures were incubated overnight at 30°C with enzyme reaction mixture at enzyme-substrate (E:S) ratios of 1:2.8, 1:5, and 1:10 (vol/vol). Cleavage reactions were quenched with sodium dodecyl sulfate (SDS) gel load-

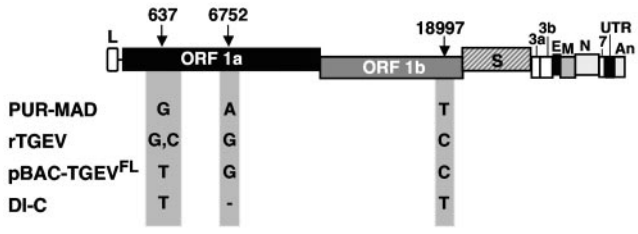

FIG. 2. Analysis of genetic markers of rTGEV viruses recovered from cDNA. The genetic structure of the TGEV cDNA clone and the positions of the genetic markers (indicated by arrows) are illustrated. Abbreviations are as in Fig. 1. The nucleotide sequence of the genetic markers is indicated for the parental virus (PUR-MAD), the rescued recombinant virus (rTGEV), the cDNA clone (pBAC-TGEV^{FL}), and the minigenome from which it was engineered (DI-C).

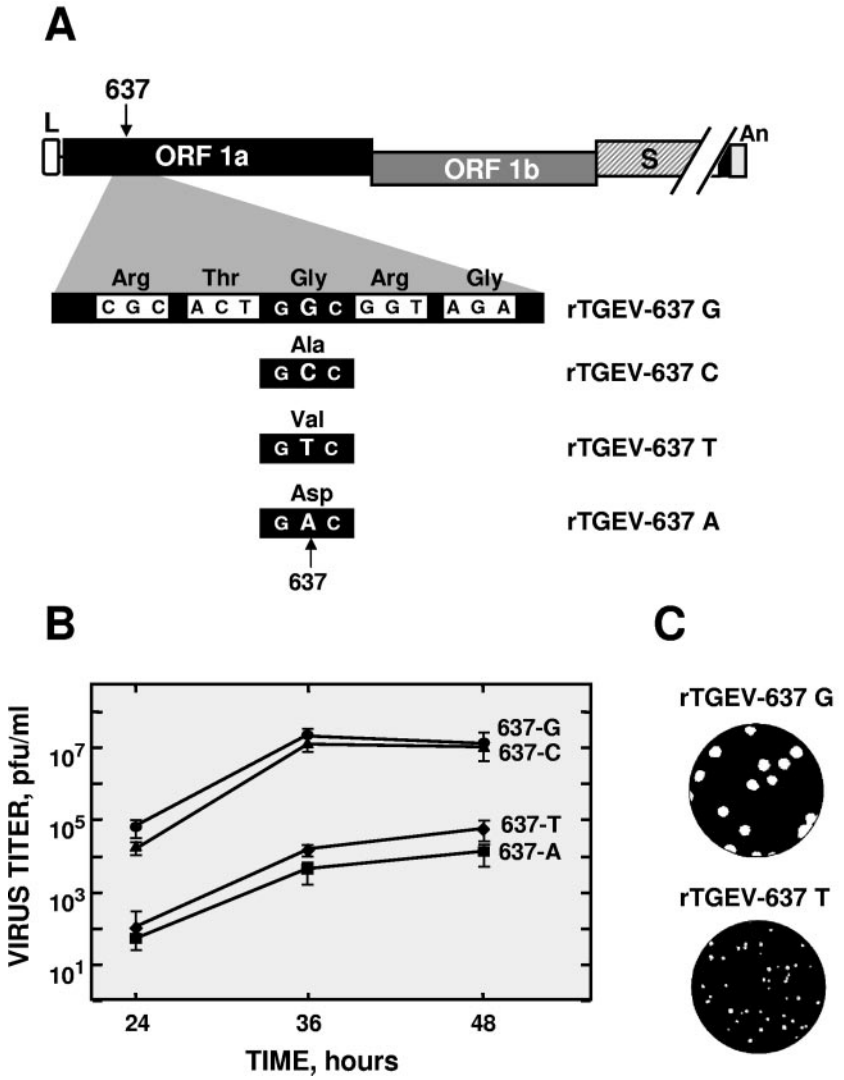

FIG. 3. Phenotype of recombinant viruses with point mutations at position 637. (A) Schematic diagram showing the genome organization of the TGEV cDNA constructs with the four nucleotide substitutions at position 637. Nucleotide substitutions and the resulting amino acid changes are indicated. The names of the recombinant viruses are indicated on the right side of the panel. (B) Virus rescue. TGEV cDNAs with the desired mutations at position 637 were transfected into BHK-pAPN cells as described in Materials and Methods and virus titers were determined at the indicated times posttransfection by plaque assay on ST cells. (C) Plaque morphology of the recombinant viruses. The phenotypes of rTGEV-637C and rTGEV-637A were similar to those of rTGEV-637G and rTGEV-637T, respectively.

ing buffer, and loaded onto SDS-10% polyacrylamide gels. After electrophoresis, gels were fixed in a methanol-acetic acid-water solution (5:1:4 [vol/vol/vol]) for 30 min, incubated in Amplify solution (Amersham NAMP100) for an additional 30 min, vacuum dried, and exposed to Kodak X-OMAT AR films at −80°C.

RESULTS

Reversion of a genetic marker in the recombinant TGEV at genome position 637. The TGEV cDNA clone pBAC-TGEV^{FL} was constructed from a defective minigenome (DI-C) derived from the respiratory strain PUR46-MAD (Fig. 1) (1). The pBAC-TGEV^{FL} construct contains two silent genetic markers at positions 6752 and 18997. A new cDNA clone containing one additional marker at position 637, which produces a conservative amino acid change (Gly to Val), was constructed (Fig. 2) because this nucleotide substitution was present in the defective minigenome DI-C and in the DI-C-derived M33L minigenomes, which are stably and efficiently replicated by the helper virus (Fig. 1). Interestingly, when the genetic markers were sequenced in different recombinant TGEV (rTGEV) clones recovered from three independent cDNA transfections, all markers were maintained except nucleotide 637, which was replaced by the parental virus sequence G or by C, supporting the idea of the existence of a strong selective pressure on position 637, suggesting that either an RNA motif or a protein mapping within this domain had been affected and was playing an important role in the virus life cycle.

Mutations at genome position 637 severely affected virus recovery from the TGEV cDNA. To analyze the role of nucleotide 637 in virus replication, the influence of point mutations at this position on virus rescue was studied by mutational analysis

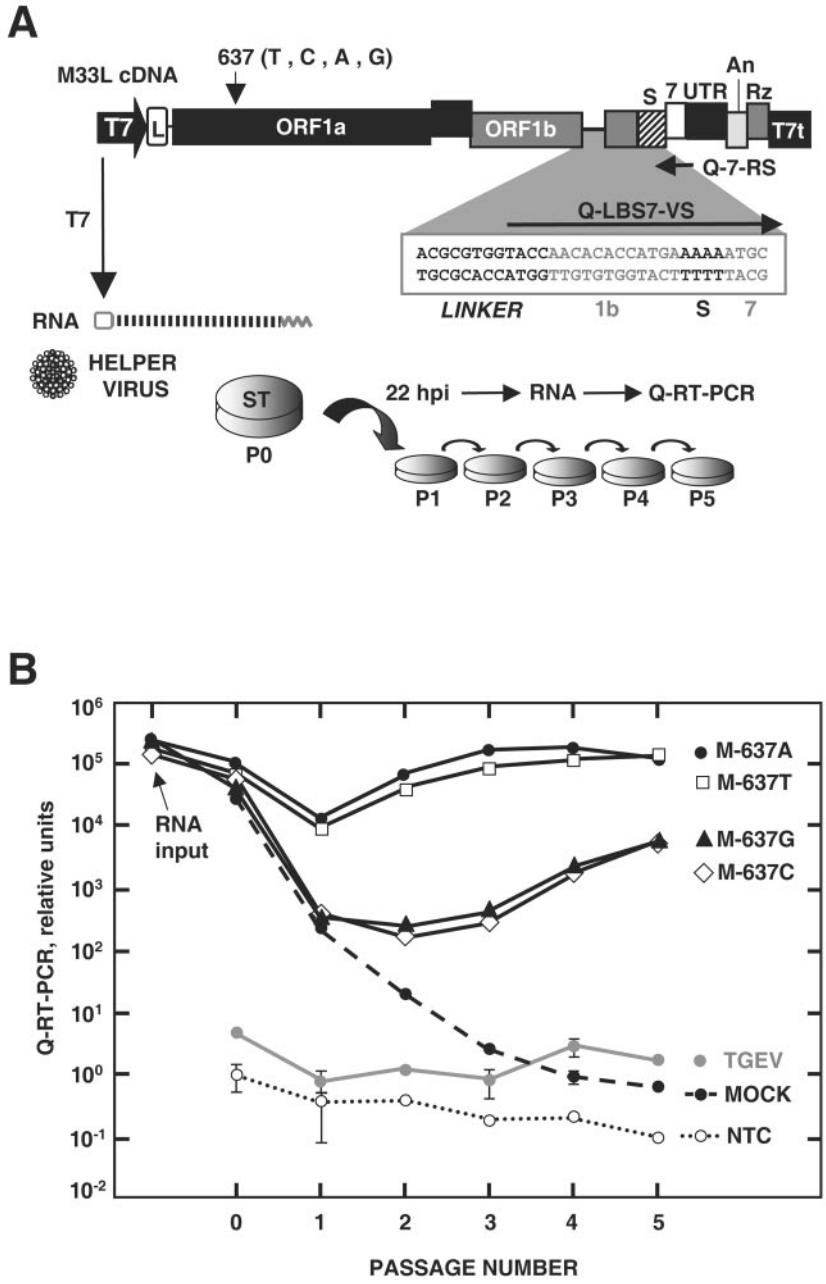

FIG. 4. Rescue of M33L mutants. (A) Scheme of the experimental procedure used to evaluate minigenome amplification. The bar on top represents the M33L cDNA, in which nucleotide 637 and the mutations introduced at this position are indicated. The discontinuous viral regions used for the specific design of the forward primer for Q-RT-PCR quantification are amplified under the M33L scheme. The specific oligonucleotides are indicated by arrows. T7-driven transcripts were transfected to helper TGEV-infected ST cells and amplified by five serial virus passages in confluent ST cell monolayers (P0 to P5). Total RNA was extracted from each virus passage to analyze minigenome amplification by Q-RT-PCR. Abbreviations are as in Fig. 1. T7, T7 promoter; Rz, ribozyme of hepatitis delta virus; T7t, T7 transcription termination signal. (B) Q-RT-PCR analysis. The RNA accumulation of M33L minigenome mutants at the successive viral passages, expressed in relative units, was determined by Q-RT-PCR. M33L-637 mutants are indicated at the right of each curve, named by the letter M followed by the corresponding mutation. Q-RT-PCR analyses of a noninfected (MOCK), a nontransfected (TGEV), and a nontemplated (NTC) control are also represented. RNA input indicates the quantification of a duplicate sample of each RNA transfection extracted at 4 h posttransfection. The standard deviation of replicate quantifications (when significant) is indicated by error bars.

using the infectious cDNA clone. Nucleotide substitution of the TGEV consensus sequence G at position 637 with C, T, or A produces an amino acid change at position 108 of the pp1a polyprotein from Gly to Ala, Val, or Asp, respectively (Fig. 3A). Recovered rTGEV viruses with the desired mutations at this position were analyzed after transfection of the corresponding TGEV cDNAs. Virus rescue was analyzed by titration (Fig. 3B), showing a reduction of three logarithmic units for recombinant viruses with T or A at position 637, which correlated with smaller plaque morphology in relation to

that of the wild type (Fig. 3C). This phenotype was not stable and revertant viruses rapidly arose at early times posttransfection, resulting in fully revertant populations after the first viral passage. No differences in virus recovery efficiency or plaque size were observed between viruses containing C or G at this position. A correlation was found between mutations 637A and 637T, causing more drastic amino acid substitutions, and the recombinant viruses affected in replication, suggesting that the effect of these point mutations was most likely at the protein level.

Effect of mutations at position 637 on minigenome rescue efficiency. In contrast to the viral genome, TGEV-derived minigenomes that are stably and efficiently replicated by the helper virus contained a T at position 637 (Fig. 1) (20). To study the relevance of nucleotide substitutions at position 637 on minigenome replication, M33L minigenome mutants at this position were generated and their ability to be replicated and packaged by the PUR46-MAD helper virus was tested. ST cells were infected with TGEV PUR46-MAD at a multiplicity of infection of 10 and transfected with T7-driven transcripts of the M33L minigenome mutants. Supernatants from these cultures were passed five times into fresh ST cells in order to amplify the minigenomes (Fig. 4A). Total RNA was extracted at each passage and minigenome rescue efficiency was determined by Q-RT-PCR using specific primers (Fig. 4A and Table 1).

To determine if differences in RNA transfection efficiency could affect minigenome rescue, M33L minigenome transfections were performed in duplicate and total RNA was extracted from one duplicate sample at 4 h posttransfection and considered the RNA input. The amount of RNA input for each M33L mutant was quantified by Q-RT-PCR and no significant differences were detected (Fig. 4B). The relative rescue ability of M33L minigenomes was determined by Q-RT-PCR and was expressed as the relative amount of RNA accumulated at each viral passage (Fig. 4B). A control of cells transfected with the M33L minigenome but not infected with the helper virus was also quantified and considered the background level (Fig. 4B, MOCK). Nonspecific hybridization of the primers with the viral genome alone was monitored using an infected and mock-transfected control to assess the specificity of the assay (Fig. 4B, TGEV). The results revealed that only M33L minigenomes with A or T at position 637 were efficiently rescued. In contrast, as indicated above, nucleotide G or C at position 637 was required for efficient virus rescue from the TGEV infectious cDNA.

Interestingly, an increase in RNA accumulation was observed after the third viral passage for both M33L-637G and M33L-637C, suggesting a genotypic reversion at position 637. To examine this possibility, the entire M33L-637G and M33L-637C minigenomes were amplified from passage five by RT-PCR and sequenced. Both M33L-637G and M33L-637C minigenomes presented genotypic reversion, with the unique nucleotide substitution at position 637 from C or G to A. These results indicate that (i) basal levels of RNA amplification allowed the selection of revertants at position 637, (ii) this single nucleotide was responsible for the observed phenotypes, and (iii) T or A was clearly preferred at position 637 for minigenome rescue by the helper virus.

Additionally, to determine if differences in virus titers during the serial passages could be responsible for the differences observed in minigenome rescue, cell culture supernatants of each virus passage were titrated on ST cells. No differences in virus titers were observed that could explain the wide differences in minigenome amplification (data not shown).

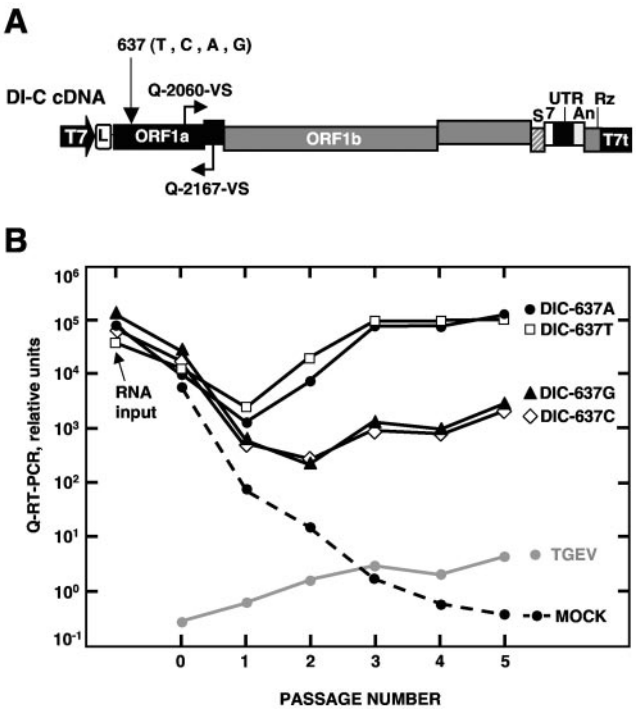

FIG. 5. Rescue of DI-C mutants. (A) Scheme of DI-C cDNA in which nucleotide 637 and the specific oligonucleotides designed to amplify the first discontinuous genomic region are indicated by arrows. Abbreviations are as in Fig. 4. (B) RNA quantification. The RNA accumulation of DI-C mutants at the successive viral passages, represented in relative units, was analyzed by Q-RT-PCR. Analyses of noninfected (MOCK) and nontransfected (TGEV) controls are also represented. RNA input indicates the quantification of a duplicate sample of each RNA transfection extracted at 4 h posttransfection. The standard deviation of replicate quantifications (when significant) is indicated by error bars.

Minigenome sequence requirements at position 637 are independent of minigenome size. The results shown above indicate that different sequence requirements at position 637 were necessary for efficient virus recovery from the infectious TGEV cDNA and for M33L minigenome rescue. Nevertheless, this observation could be a unique feature of the M33L minigenome or a general requirement for any TGEV-derived minigenome amplification. To extend our studies to a minigenome of a different size, the TGEV defective interfering RNA DI-C of 9.7 kb (Fig. 1) was used to perform a similar mutational analysis. ST cells were infected and transfected with the corresponding DI-C mutants and RNA accumulation was quantified by Q-RT-PCR for each virus passage using the same procedure and quantification controls as described for the M33L mutants (Fig. 5B). DI-C minigenomes containing T or A at position 637 were efficiently rescued, whereas DI-C mutants presenting G or C at the same position were severely affected in their ability to be rescued, showing the same behavior as the corresponding mutants of the M33L minigenome. On the basis of these results, it can be concluded that the same sequence requirements at nucleotide 637 are necessary for amplification

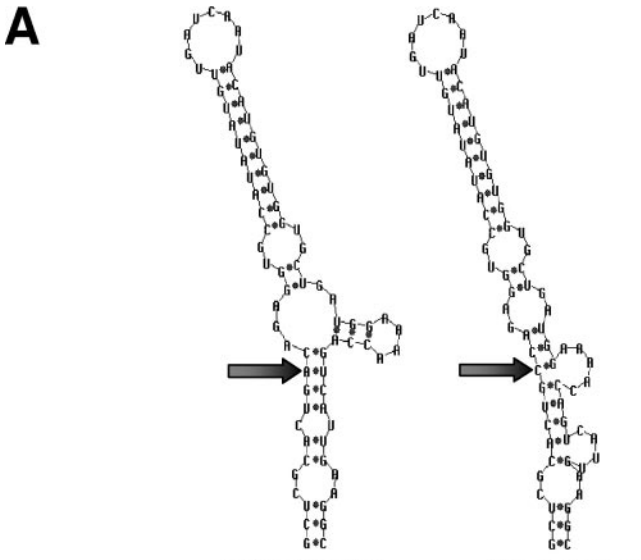

B

CONSTRUCT	nt	aa	RNA FOLDING	REPLICATION
rTGEV-637 G	G	Gly	A	+ + +
rTGEV-637 C	C	Ala	B	+ + +
rTGEV-637 T	T	Val	B	+
rTGEV-637 A	A	Asp	A	+
DIC/ M33L-637 G	G	Gly	A	-
DIC/ M33L-637 C	C	Ala	B	-
DIC/ M33L-637 T	T	Val	B	+ + +
DIC/ M33L-637 A	A	Asp	A	+ + +

FIG. 6. In silico analysis of the RNA secondary structure of the TGEV domain containing nucleotide 637. (A) Secondary structure of the RNA sequence derived from the TGEV mutants. The secondary structure was predicted for each mutant using the Mfold 3.1 software. Predicted minimum energy structures were common for sequences containing G or A at position 637 (folding A) or those containing T or C (folding B). Only the RNA motif containing nucleotide 637 is shown, with an arrow indicating the nucleotide at this position. (B) Relationship between structure predictions of the RNA domain containing each substitution for nucleotide 637 and the observed phenotypes of the viruses and minigenomes with the corresponding mutations.

of both DI-C and M33L minigenomes regardless of their different sizes.

Effect of mutations at nucleotide 637 on RNA secondary-structure predictions. Consistent with previous results, it seems that both *cis* and *trans* TGEV replication was severely affected by single mutations at nucleotide 637, and different bases at this position were required and naturally selected for efficient virus or minigenome rescue. Mutations at nucleotide position 637 produce an amino acid change at position 108 of the pp1a and pp1ab polyproteins (Fig. 3A). Mutational analysis performed with the TGEV cDNA showed that mutations causing more drastic amino acid changes correlated with those viruses that were more affected in replication. Furthermore, amino acid 108 mapped in the putative N-terminal PLP-1 cleavage site at the p9/p87 junction (Fig. 7A), as predicted by comparative sequence analysis with the human coronavirus HCoV-229E (16), suggesting that the effect of mutations at position 637 was at the protein level. Nevertheless, we cannot discard the idea that changes in the secondary structure of the RNA domain containing the nucleotide 637 could be responsible for the virus and minigenomes phenotypes.

To analyze this possibility, the relationship between the dif-

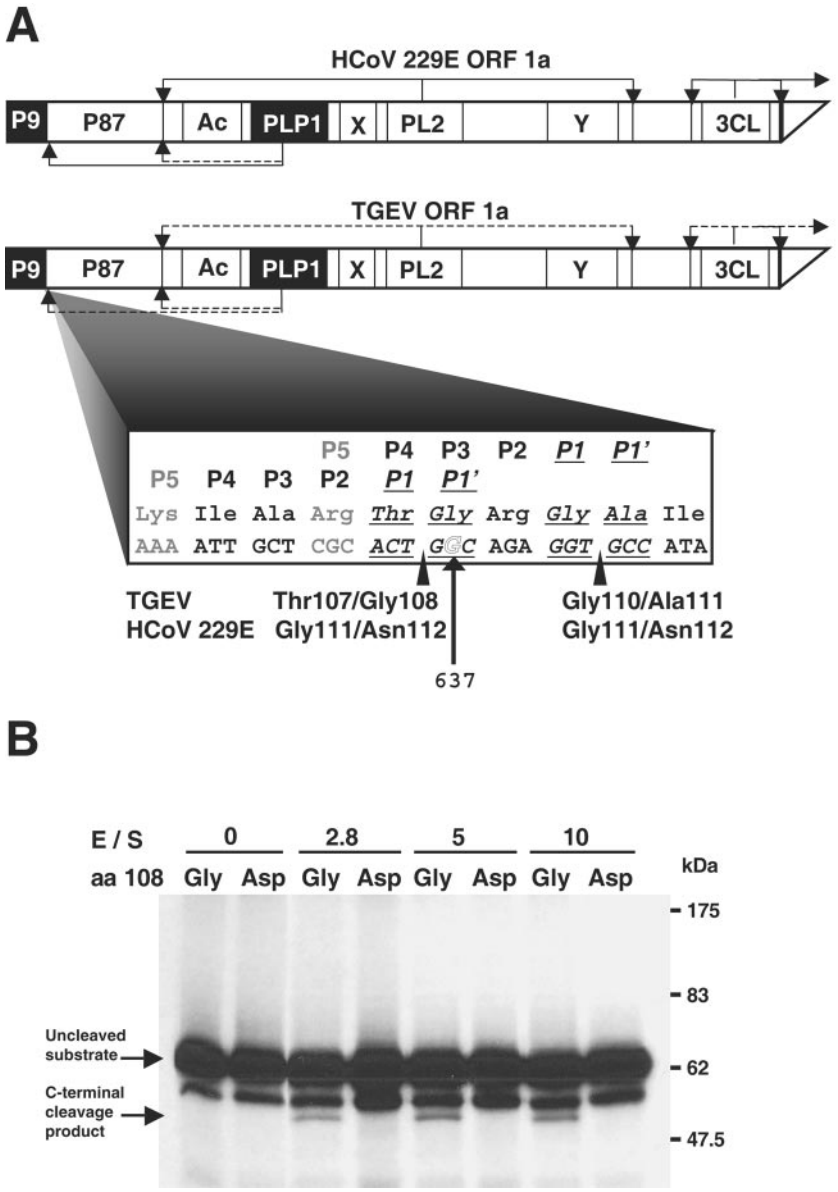

FIG. 7. Point mutations at nucleotide 637 affected N-terminal replicase processing in vitro. (A) Schematic representation of the amino-terminal region of ORF1a for HCoV-229E and TGEV. Arrows represent PLP-1 cleavage sites that have been experimentally shown (continuous lines) or inferred by sequence comparison (dotted lines). Replicase sequence containing the codon affected by mutations at position 637 is depicted. The two possible cleavage sites (black arrowheads) at the N terminus of the TGEV replicase were predicted by sequence alignment with HCoV-229E. Amino acids flanking the two potential PLP-1 cleavage sites are designated according to the nomenclature introduced by Schechter and Berger (38) as NH_2-P3-P2-P1 ↓ P1′-P2′-P3′-COOH. (B) *trans*-Cleavage assay. The PLP-1 domain and the pp1a N-terminal 610 amino acids with the wild-type sequence G at position 637 or an A at the same position, leading to the least conservative amino acid change (Gly108Asp), were generated as described in Materials and Methods. After translation, 1 volume of [^{35}S]methionine-labeled substrate was incubated for 14 h at 30°C in the absence or presence of 2.8, 5, or 10 volumes of enzyme reaction mixture. The cleavage reaction products were separated by sodium dodecyl sulfate–10% polyacrylamide gel electrophoresis and analyzed by fluorography. Molecular mass markers are given on the left in kDa, and the uncleaved substrate and C-terminal cleavage product are indicated by arrows on the right.

ferent mutations at position 637, the replication ability of the corresponding virus and minigenome mutants, and the secondary structure of the RNA domain containing this nucleotide were studied (Fig. 6B). Structure predictions were performed using the Mfold software (26, 49) and constructs derived from the 5′ end of the TGEV genome with point mutations at position 637 were analyzed. Two folding patterns were obtained, one common for constructs containing G or A at position 637 (Fig. 6A, folding A) and another one for those containing C or T at the same position (Fig. 6A, folding B). A more detailed analysis considering sequences of different lengths and both positive and negative RNA strand polarities was consistent with this observation (data not shown). As described above, different phenotypes were observed for virus or minigenomes containing G or A and for those presenting T or C. Therefore, no correlation was found between predictions of

RNA folding and virus or minigenome replication ability, supporting the idea that the effect of mutations at position 637 was most probably at the protein level.

Mutations at nucleotide 637 affected N-terminal replicase processing in vitro by PLP-1. The results reported so far point toward an effect of the mutations at position 637, associated with processing at the N-terminal region of the TGEV replicase. The PLP-1 cleavage site can occupy a variable position at the amino terminus of the replicase polyproteins, as has been reported for different coronaviruses (17, 19). The PLP-1 of HCoV-229E, closely related to TGEV coronavirus, is responsible for the release of the N-terminal p9 protein from the pp1a and pp1ab polyproteins, with cleavage occurring between residues Gly111 and Asn112 (Fig. 7A). No experimental data have been reported for TGEV polyprotein processing, although potential cleavage sites are proposed by comparative sequence analysis with HCoV-229E.

Amino acid 108, affected by mutations at nucleotide position 637, occupies the P1′ position at the Thr107/Gly108 theoretical cleavage site or the P3 position at the Gly110/Ala111 alternative cleavage site (Fig. 7A) (17). In both cases, a drastic amino acid change could probably affect the processing mediated by the PLP-1, as described in mutagenesis studies and sequence analyses of three PLP-1 cleavage sites (3, 12, 19). To support this hypothesis, a *trans*-cleavage assay was performed with the putative TGEV PLP-1 domain and an N-terminal pp1a substrate with either the wild-type sequence G at position 637 or an A at the same position, leading to the least conservative amino acid change (Gly108Asp). A fragment containing the predicted PLP-1 domain was cloned to undergo T7-driven transcription coupled to translation. An in vitro translation product representing the amino-terminal 610 amino acids of TGEV pp1a was used as the ^{35}S-labeled substrate in the *trans*-cleavage assay. This sequence was selected because it is the one encoded by the first 2,144 nucleotides present at the 5′ continuous genomic region in both M33L and DI-C minigenomes, which are efficiently rescued by the helper virus.

After translation was accomplished, different enzyme-substrate volume ratios were tested for cleavage by combining translation mixtures including the substrate and the PLP-1 (Fig. 7B). In the absence of enzyme, only the labeled substrate with a molecular mass of 67 kDa was detected, together with a minor protein band that was probably the result of premature termination events during transcription or translation. When PLP-1 was included, a processed form of the substrate was detected with the substrate containing a Gly residue at position 108, but not with that presenting an Asp residue at the same position. The PLP-1 cleavage efficiency observed was similar for the different enzyme-substrate ratios tested. The pp1a proteolytic product correlated with the expected size of the C-terminal cleavage product generated after the release of the N-terminal p9 protein, and was not the result of a spontaneous degradation event from this particular substrate, since this processed protein was not detected when both substrates were incubated in parallel without enzyme. In this experiment, no N-terminal p9 cleavage product was detected, probably due to its reduced labeling (the cleaved peptide contains only two radiolabeled residues, compared to seven present in the C-terminal cleavage product) and to a reduced efficiency of PLP-1. These results indicated that mutations at nucleotide 637 affected the in vitro cleavage of the TGEV replicase mediated by PLP-1.

DISCUSSION

The effect of point mutations at position 637, mapping at the putative N-terminal cleavage site of the TGEV replicase, on virus and minigenome replication has been characterized. Mutations at nucleotide 637 affected the in vitro cleavage of the TGEV replicase mediated by PLP-1. Different mutations at position 637 were required for virus recovery from the cDNA and minigenome accumulation. A correlation has been established between those mutations most likely interfering with proper N-terminal replicase processing and the limited rescue efficiency of the recombinant viruses.

Despite the relative flexibility of the TGEV infectious clone for genetic modification (29), a point mutation that was present in the defective interfering minigenome DI-C, which is stably and efficiently amplified in *trans* by the helper virus, was rapidly reverted in the genome of the recombinant progeny virions, indicating a strong selective pressure at this position.

The correlation between nucleotide 637 and the N-terminal cleavage of the replicase by the viral proteinase PLP-1 was based on previous sequence alignments reported for the HCoV-229E and TGEV replicase polyproteins (17). HCoV-229E PLP-1 activity and substrate specificity has been reported (16, 17). According to these studies, TGEV PLP-1 mediates N-terminal cleavage at either Thr107/Gly108 or Gly110/Ala111. Nucleotide substitutions at position 637 affect the nature of amino acid 108, which occupies the P1′ and P3 residues relative to the Thr107/Gly108 and Gly110/Ala111 cleavage sites, respectively. In this report, it has been shown that a nonconservative amino acid change at this position affected the cleavage mediated by PLP-1 using an in vitro *trans*-cleavage assay. The processing of PLP-1 was limited, as previously described for in vitro assays with minimal domains of coronavirus PLP proteinases acting in *trans* (16, 41). These results could be due to the relatively reduced length of the substrate, to the lack of flanking domains required for efficient processing in the PLP-1 construct tested (47), or both.

The effect of mutations at position 637 was studied in two systems, the full-length TGEV genome and TGEV-derived defective minigenomes. The introduction of mutations predictably affecting proper replicase processing in the full-length TGEV genome caused a dramatic reduction in the virus recovery and a small-plaque-size phenotype, suggesting a critical role in virus replication of the proteins related to this cleavage site. PLP-1 cleavage products have been identified in virus-infected cells for HCoV-229E coronavirus, such as an early-released p9 polypeptide, a p87 adjacent protein, and several polypeptides with apparent molecular masses of 93 kDa (p93), 170 kDa (p170), and 230 kDa (p230), whose identity and potential precursor-product relationships remain to be determined (16). However, no functional data have been reported so far for these proteins and there is no obvious sequence comparison from which a putative function could be deduced.

The equivalent proteins of MHV replicase are generated from a relatively divergent amino-terminal domain. Thus, the p28 and p65 polypeptides are the counterparts of the p9 and p87 proteins of HCoV-229E, respectively. Biochemical studies have shown that the MHV p28 and p65 polypeptides seem to

be associated with intracellular membranes and colocalize with viral replication complexes (6, 39). In addition, recent data correlated p28 expression with cell cycle arrest in G_0/G_1 phase (8). Our data correlated with the mutational analysis performed in the MHV-A59 infectious clone at the N-terminal PLP-1 cleavage site of the MHV replicase, in which predicted noncleaving mutations severely affected virus growth, protein processing, and RNA synthesis (11). However, in contrast to the MHV mutants, the TGEV mutants characterized in our work harboring predicted noncleaving mutations were not stable and could not be characterized further, since rapidly reverted to the wild-type sequence. Although group-specific divergences could explain different requirements at this cleavage site, it seems clear that the abrogation of this specific processing event severely compromises the virus viability for both the MHV and TGEV coronaviruses.

In contrast, TGEV-derived minigenomes with predicted noncleaving mutations at the N-terminal cleavage site were efficiently rescued by the helper virus, whereas predicted cleaving mutations negatively affected their ability to be rescued in *trans*. The observed differences might have relevant implications. (i) Sequence requirements for minigenome amplification in *trans* could differ from those required for genome replication in *cis*, reinforcing the need to generate replicons to study coronavirus replication instead of using defective minigenomes. (ii) Different mechanisms seem to operate in the replication of full-length viral genomes and minigenomes, allowing the minigenomes to take advantage of the replication machinery of the helper virus to modulate viral infectivity. (iii) The defective minigenomes M33L and DI-C encode a replicase-derived fusion protein that could interfere with minigenome amplification due to the different mature products generated after processing. This fusion protein comprises the first 610 amino acids from the replicase N terminus, merged in phase with the last 58 amino acids of pp1a, and the slippery sequence that could produce the translation frameshift resulting in a extended version of this fusion protein.

Although there is no consensus about the translation requirements of the defective coronavirus RNAs characterized so far, it seems that translation, not the encoded sequence, might confer an advantage for the efficient propagation of these RNAs, most probably by coupling the translation and replication mechanisms (22, 24, 43). The putative cleavage of this fusion protein in the minigenomes studied, M33L and DI-C, by the helper virus PLP-1 proteinase activity would release the amino-terminal p9 polypeptide and a fusion protein containing a truncated form of the p87 polypeptide. A plausible interpretation is that the truncated polypeptide might interfere with minigenome amplification by sequestering the minigenome in nonfunctional replication complexes, interfering with the access of the minigenome to the helper virus replication machinery. Further experiments will be required to characterize the strategy developed by minigenomes to undergo effective *trans*-amplification and the specific function of each component of coronavirus replicase polyproteins in the synthesis of the different species of viral RNA.

ACKNOWLEDGMENTS

We thank S. Zúñiga for critically reading the manuscript and helpful discussions.

This work was supported by grants from the Ministerio de Educación y Ciencia (MEC) of Spain, Fort Dodge Veterinaria, and the European Community (Frame V, Key Action 2, Control of Infectious Disease Projects QLRT-2000-00874, and Frame VI, SP22-CT-2004-511060). C.G. received a predoctoral fellowship from the MEC.

REFERENCES

1. **Almazán, F., J. M. González, Z. Pénzes, A. Izeta, E. Calvo, J. Plana-Durán, and L. Enjuanes.** 2000. Engineering the largest RNA virus genome as an infectious bacterial artificial chromosome. Proc. Natl. Acad. Sci. USA **97:** 5516–5521.
2. **Baker, S. C., C. K. Shieh, L. H. Soe, M. F. Chang, D. M. Vannier, and M. M. C. Lai.** 1989. Identification of a domain required for autoproteolytic cleavage of murine coronavirus gene A polyprotein. J. Virol. **63:**3693–3699.
3. **Bonilla, P. J., S. A. Hughes, and S. R. Weiss.** 1997. Characterization of a second cleavage site and demonstration of activity in trans by the papain-like proteinase of the murine coronavirus mouse hepatitis virus strain A59. J. Virol. **71:**900–909.
4. **Brian, D. A., and R. S. Baric.** 2005. Coronavirus genome structure and replication. Curr. Top. Microbiol. Immunol. **287:**1–30.
5. **Brierley, I., P. Digard, and S. C. Inglis.** 1989. Characterization of an efficient coronavirus ribosomal frameshifting signal: requirement for an RNA pseudoknot. Cell **57:**537–547.
6. **Brockway, S. M., X. T. Lu, T. R. Peters, T. S. Dermody, and M. R. Denison.** 2004. Intracellular localization and protein interactions of the gene 1 protein p28 during mouse hepatitis virus replication. J. Virol. **78:**11551–11562.
7. **Cavanagh, D., D. A. Brian, P. Britton, L. Enjuanes, M. C. Horzinek, M. M. C. Lai, H. Laude, P. G. W. Plagemann, S. Siddell, W. Spaan, and P. J. Talbot.** 1997. *Nidovirales*: a new order comprising *Coronaviridae* and *Arteriviridae*. Arch. Virol. **142:**629–635.
8. **Chen, C. J., K. Sugiyama, H. Kubo, C. Huang, and S. Makino.** 2004. Murine coronavirus nonstructural protein p28 arrests cell cycle in G_0/G_1 phase. J. Virol. **78:**10410–10419.
9. **Delmas, B., J. Gelfi, H. Sjöström, O. Noren, and H. Laude.** 1993. Further characterization of aminopeptidase-N as a receptor for coronaviruses. Adv. Exp. Med. Biol. **342:**293–298.
10. **Denison, M. R., S. A. Hughes, and S. R. Weiss.** 1995. Identification and characterization of a 65-kDa protein processed from the gene 1 polyprotein of the murine coronavirus MHV-A59. Virology **207:**316–320.
11. **Denison, M. R., B. Yount, S. M. Brockway, R. L. Graham, A. C. Sims, X. Lu, and R. S. Baric.** 2004. Cleavage between replicase proteins p28 and p65 of mouse hepatitis virus is not required for virus replication. J. Virol. **78:**5957–5965.
12. **Dong, S., and S. Baker.** 1994. Determinants of the p28 cleavage site recognized by the first papain-like cysteine proteinase of murine coronavirus. Virology **204:**541–549.
13. **Drosten, C., S. Günther, W. Preiser, S. van der Werf, H. R. Brodt, S. Becker, H. Rabenau, M. Panning, L. Kolesnikova, R. A. M. Fouchier, A. Berger, A. M. Burguiere, J. Cinatl, M. Eickmann, N. Escriou, K. Grywna, S. Kramme, J. C. Manuguerra, S. Muller, W. Rickerts, M. V. Sturmer, S., H. D. Klenk, and A. D. M. E. Osterhaus.** 2003. Identification of a novel coronavirus in patients with severe acute respiratory syndrome. N. Engl. J. Med. **348:** 1967–1976.
14. **Enjuanes, L., W. Spaan, E. Snijder, and D. Cavanagh.** 2000. *Nidovirales*, p. 827–834. *In* R. B. Wickner (ed.), Virus taxonomy: classification and nomenclature of viruses. Academic Press, San Diego, Calif.
15. **Esper, F., C. Weibel, D. Ferguson, M. L. Landry, and J. S. Kahn.** 2005. Evidence of a novel human coronavirus that is associated with respiratory tract disease in infants and young children. J. Infect. Dis. **191:**492–498.
16. **Herold, J., A. E. Gorbalenya, V. Thiel, B. Schelle, and S. G. Siddell.** 1998. Proteolytic processing at the amino terminus of human coronavirus 229E gene 1-encoded polyproteins: identification of a papain-like proteinase and its substrate. J. Virol. **72:**910–918.
17. **Herold, J., V. Thiel, and S. G. Siddell.** 1998. Characterization of a papain-like cysteine-proteinase encoded by gene 1 of the human coronavirus HCV 229E. Adv. Exp. Med. Biol. **440:**141–148.
18. **Hofmann, M. A., P. B. Sethna, and D. A. Brian.** 1990. Bovine coronavirus mRNA replication continues throughout persistent infection in cell culture. J. Virol. **64:**4108–4114.
19. **Hughes, S. A., P. J. Bonilla, and S. R. Weiss.** 1995. Identification of the murine coronavirus p28 cleavage site. J. Virol. **69:**809–813.
20. **Izeta, A., C. Smerdou, S. Alonso, Z. Penzes, A. Méndez, J. Plana-Durán, and L. Enjuanes.** 1999. Replication and packaging of transmissible gastroenteritis coronavirus-derived synthetic minigenomes. J. Virol. **73:**1535–1545.
21. **Jiménez, G., I. Correa, M. P. Melgosa, M. J. Bullido, and L. Enjuanes.** 1986. Critical epitopes in transmissible gastroenteritis virus neutralization. J. Virol. **60:**131–139.
22. **Kim, Y. N., M. M. C. Lai, and S. Makino.** 1993. Generation and selection of coronavirus defective interfering RNA with large open reading frame by RNA recombination and possible editing. Virology **194:**244–253.
23. **Lai, M. M. C., and D. Cavanagh.** 1997. The molecular biology of coronaviruses. Adv. Virus Res. **48:**1–100.

24. **Liao, C. L., and M. M. Lai.** 1995. A cis-acting viral protein is not required for the replication of a coronavirus defective-interfering RNA. Virology **209:** 428–436.
25. **Makino, S., F. Taguchi, and K. Fujiwara.** 1984. Defective interfering particles of mouse hepatitis virus. Virology **133:**9–17.
26. **Mathews, D. H., J. Sabina, M. Zuker, and D. H. Turner.** 1999. Expanded sequence dependence of thermodynamic parameters improves prediction of RNA secondary structure. J. Mol. Biol. **288:**911–940.
27. **McClurkin, A. W., and J. O. Norman.** 1966. Studies on transmissible gastroenteritis of swine. II. Selected characteristics of a cytopathogenic virus common to five isolates from transmissible gastroenteritis. Can. J. Comp. Med. Vet. Sci. **30:**190–198.
28. **Méndez, A., C. Smerdou, A. Izeta, F. Gebauer, and L. Enjuanes.** 1996. Molecular characterization of transmissible gastroenteritis coronavirus defective interfering genomes: packaging and heterogeneity. Virology **217:**495–507.
29. **Ortego, J., I. Sola, F. Almazan, J. E. Ceriani, C. Riquelme, M. Balasch, J. Plana-Durán, and L. Enjuanes.** 2003. Transmissible gastroenteritis coronavirus gene 7 is not essential but influences *in vivo* virus replication and virulence. Virology **308:**13–22.
30. **Penzes, Z., J. M. González, E. Calvo, A. Izeta, C. Smerdou, A. Mendez, C. M. Sánchez, I. Sola, F. Almazán, and L. Enjuanes.** 2001. Complete genome sequence of transmissible gastroenteritis coronavirus PUR46-MAD clone and evolution of the Purdue virus cluster. Virus Genes **23:**105–118.
31. **Penzes, Z., K. Tibbles, K. Shaw, P. Britton, T. D. K. Brown, and D. Cavanagh.** 1994. Characterization of a replicating and packaged defective RNA of avian coronavirus infectious bronchitis virus. Virology **203:**286–293.
32. **Perlman, S., T. E. Lane, and M. J. Buchmeier.** 2000. Coronavirus: hepatitis, peritonitis, and central nervous system disease, p. 331–348. *In* R. S. Fujinami (ed.), Effects of microbes on the immune system. Lippincott Williams and Wilkins, Philadelphia, Pa.
33. **Qiu, W., J. W. Park, A. O. Jackson, and H. B. Scholthof.** 2001. Retention of a small replicase gene segment in tomato bushy stunt virus defective RNAs inhibits their helper-mediated trans-accumulation. Virology **281:**51–60.
34. **Rota, P. A., M. S. Oberste, S. S. Monroe, W. A. Nix, R. Campganoli, J. P. Icenogle, S. Peñaranda, B. Bankamp, K. Maher, M. H. Chen, S. Tong, A. Tamin, L. Lowe, M. Frace, J. L. DeRisi, Q. Chen, D. Wang, D. d. Erdman, T. C. T. Peret, C. Burns, T. G. Ksiazek, P. E. Rollin, A. Sanchez, S. Liffick, B. Holloway, J. Limor, K. McCaustland, M. Olsen-Rassmussen, R. Fouchier, S. Gunther, A. D. M. E. Osterhaus, C. Drosten, M. A. Pallansch, L. J. Anderson, and W. J. Bellini.** 2003. Characterization of a novel coronavirus associated with severe acute respiratory syndrome. Science **300:**1394–1399.
35. **Sánchez, C. M., G. Jiménez, M. D. Laviada, I. Correa, C. Suñé, M. J. Bullido, F. Gebauer, C. Smerdou, P. Callebaut, J. M. Escribano, and L. Enjuanes.** 1990. Antigenic homology among coronaviruses related to transmissible gastroenteritis virus. Virology **174:**410–417.
36. **Sawicki, S. G., and D. L. Sawicki.** 2005. Coronavirus transcription: a perspective. Curr. Top. Microbiol. Immunol. **287:**31–55.
37. **Sawicki, S. G., and D. L. Sawicki.** 1998. A new model for coronavirus transcription. Adv. Exp. Med. Biol. **440:**215–220.
38. **Schechter, I., and A. Berger.** 1967. On the size of the active site in proteases. I. Papain. Biochem. Biophys. Res. Commun. **27:**157–162.
39. **Sims, A. C., J. Ostermann, and M. R. Denison.** 2000. Mouse hepatitis virus replicase proteins associate with two distinct populations of intracellular membranes. J. Virol. **74:**5647–5654.
40. **Sola, I., J. L. Moreno, S. Zúñiga, S. Alonso, and L. Enjuanes.** 2005. Role of nucleotides immediately flanking the transcription-regulating sequence core in coronavirus subgenomic mRNA synthesis. J. Virol. **79:**2506–2516.
41. **Teng, H., J. D. Pinon, and S. R. Weiss.** 1999. Expression of murine coronavirus recombinant papain-like proteinase: efficient cleavage is dependent on the lengths of both the substrate and the proteinase polypeptides. J. Virol. **73:**2658–2666.
42. **van der Hoek, L., K. Pyrc, M. F. Jebbink, W. Vermeulen-Oost, R. J. Berkhout, K. C. Wolthers, P. M. Wertheim-van Dillen, J. Kaandorp, J. Spaargaren, and B. Berkhout.** 2004. Identification of a new human coronavirus. Nat. Med. **10:**368–373.
43. **van der Most, R., W. Luytjes, S. Rutjes, and W. J. M. Spaan.** 1995. Translation but not the encoded sequence is essential for the efficient propagation of the defective interfering RNAs of the coronavirus mouse hepatitis virus. J. Virol. **69:**3744–3751.
44. **van der Most, R. G., P. J. Bredenbeek, and W. J. M. Spaan.** 1991. A domain at the 3′ end of the polymerase gene is essential for encapsidation of coronavirus defective interfering RNAs. J. Virol. **65:**3219–3226.
45. **Woo, P. C., S. K. Lau, C. M. Chu, K. H. Chan, H. W. Tsoi, Y. Huang, B. H. Wong, R. W. Poon, J. J. Cai, W. K. Luk, L. L. Poon, S. S. Wong, Y. Guan, J. S. Peiris, and K. Y. Yuen.** 2005. Characterization and complete genome sequence of a novel coronavirus, coronavirus HKU1, from patients with pneumonia. J. Virol. **79:**884–895.
46. **Ziebuhr, J.** 2005. The coronavirus replicase. Curr. Top. Microbiol. Immunol. **287:**57–94.
47. **Ziebuhr, J., E. J. Snijder, and A. E. Gorbalenya.** 2000. Virus-encoded proteinases and proteolytic processing in the *Nidovirales*. J. Gen. Virol. **81:**853–879.
48. **Ziebuhr, J., V. Thiel, and A. E. Gorbalenya.** 2001. The autocatalytic release of a putative RNA virus transcription factor from its polyprotein precursor involves two paralogous papain-like proteases that cleave the same peptide bond. J. Biol. Chem. **276:**33220–33232.
49. **Zuker, M.** 2003. Mfold web server for nucleic acid folding and hybridization prediction. Nucleic Acids Res. **31:**3406–3415.
50. **Zúñiga, S., I. Sola, S. Alonso, and L. Enjuanes.** 2004. Sequence motifs involved in the regulation of discontinuous coronavirus subgenomic RNA synthesis. J. Virol. **78:**980–994.